

In preparation for the Astrophysical Journal

Analysis of Four A-F Supergiants in M31 from Keck HIRES Spectroscopy ¹

K. A. Venn^{2,3}

Macalester College, Saint Paul, MN, 55105

J. K. McCarthy⁴

Palomar Observatory, California Institute of Technology, Pasadena, CA, 91125

D. J. Lennon²

Isaac Newton Group of Telescopes (ING), Santa Cruz de La Palma, Canary Islands,
E-38780, Spain

N. Przybilla and R. P. Kudritzki⁵

Institut für Astronomie und Astrophysik, Universität Sternwarte München, München,
D-81679, Germany

and

M. Lemke⁶

Dr. Karl Remeis-Sternwarte, Bamberg, D-96049, Germany

ABSTRACT

¹Based on observations obtained at the W.M. Keck Observatory, which is operated as a scientific partnership among the California Institute of Technology, the University of California, and the National Aeronautics and Space Administration. The Observatory was made possible by the generous financial support of the W.M. Keck Foundation.

²Institut für Astronomie und Astrophysik, Universität Sternwarte München, Scheinerstrasse 1, München, D-81679, Germany

³Adjunct Assistant Professor, Department of Astronomy, University of Minnesota, Minneapolis, MN, 55455

⁴Present address: Pixel Vision, Inc., Advanced Imaging Sensors Division, 4952 Warner Avenue, Suite 300, Huntington Beach, CA, 92649

⁵Max Planck Institut für Astrophysik, Garching, D-85740, Germany

⁶Present address: INA-Werk Schaeffler, Herzogenaurach, Germany

The first stellar abundances in M31 are presented, based on Keck I HIRES spectroscopy and model atmospheres analyses of three A-F supergiants, 41-2368, 41-3712, and A-207. We also present the preliminary analysis of a fourth star, 41-3654. We find that the stellar oxygen abundances are in good agreement with those determined from nebular studies, even though the stars do *not* show a clear radial gradient in oxygen. The uncertainties in the stellar abundances are smaller than the range in the nebular results, making these stars ideal objects for further studies of the distribution of oxygen in M31. We show that the stars can be used to study the abundance distributions of other elements as well, including iron-group and heavier elements.

The A-F supergiants also provide direct information on the metallicity and reddening of nearby Cepheid stars. We have examined the metallicity and reddening assumptions used for Cepheids within 1' of our targets and noted the differences from values used in the literature.

Subject headings: stars: abundances, atmospheres, supergiants — galaxies: abundances, individual (M31), stellar content

1. Introduction

Light element abundances in the disk of M31 are known primarily from nebular analyses of H II regions and supernovae remnants (Blair *et al.* 1981, 1982, Dennefeld & Kunth 1981), and more recently from a few disk planetary nebulae (2 PNe by Jacoby & Ciardullo 1999, 3 by Jacoby & Ford 1986, and 2 by Richer *et al.* 1999). The nebular abundances have identified a mild gradient in oxygen with galactocentric distance, with a fairly large range in the abundances at a given radial distance. Until recently, the stars in M31 have been too faint to observe with high resolution spectroscopy for detailed atmospheric analyses. The advent of large telescopes and efficient detectors is changing this though, and now high resolution spectroscopy of stars fainter than $V=17$ can be obtained, making stellar atmospheric analyses of stars beyond the Magellanic Clouds a new possibility.

One question that new elemental abundances from stars can address concerns abundance gradients that are commonly identified in spiral galaxies (surveys of H II regions in numerous spiral galaxies have been carried out by McCall *et al.* 1985, Vila-Costas & Edmunds 1992, and Zaritsky *et al.* 1994). While there is no doubt about the existence of these gradients in many galaxies, it is the exact form of the gradient, the dispersion in abundance at a given galactocentric radial distance, and the constancy of the gradient

between different elements, that new stellar studies can address. And, in contrast to abundance determinations using H II regions, which provide information mainly on light elements (e.g., He, N and O), stellar analyses can provide the abundances of these and heavier elements (e.g., O, Mg, Fe, and possibly even Ba). Through the study of these additional elements, new insights will be gained into the nucleosynthetic history and chemical evolution of spiral galaxies.

Stellar atmosphere analyses are also relevant to Cepheid distance determinations, through metallicity calculations and reddening estimates. As the accuracy in the determination of H_0 reaches the stated HST Key Project goal of 10% (Kennicutt, Freedman, & Mould 1995), then the systematic uncertainties in the Cepheid distances themselves become increasingly important. In particular, the question of metallicity effects on the Cepheid period-luminosity (PL) relationship, and uncertainties in the reddening estimates (c.f., Kennicutt *et al.* 1998). The A-F supergiants are physically linked to Cepheids; these stars have similar young ages and intermediate-masses, and should have very similar compositions and galactic (thin disk) locations. The element ratios (e.g, O/Fe) found from the A-F supergiants can be used for the most accurate metallicity/opacity studies of Cepheids, e.g., simple scaling of the oxygen abundances from nebular analyses to all other elements does not allow for differences due to the chemical evolution history of different galaxies. The similar locations of A-F supergiants and Cepheids also mean that reddening estimates can be checked or improved (i.e., after detailed atmospheric analyses of the A-F supergiants).

In this paper, we present the first elemental abundances from high resolution stellar spectroscopy of individual stars in M31. Model atmospheres analyses for three A-F supergiants are presented, as well as preliminary results for a fourth star. The elements observed include alpha-elements (O, Mg, Si, Ca, Ti) as well as iron-group elements (Cr, Fe, Ni), and the first heavy element abundances (Y, Ba, Ce, Nd) for M31. The oxygen abundances are compared to the nebular radial gradient, and we discuss the importance of examining other elemental gradients as well as element ratios to study the chemical evolution of the disk of M31. We also determine reddening to the A-F supergiants, and compare the adopted reddening and metallicity estimates of nearby Cepheids to discuss potential improvements in the Cepheid distance determinations.

2. Observations and Reductions

Observations of three A-type supergiants (41-3712, 41-2368, and 41-3654) in M31 were taken on August 1, 1995, with the 10 m Keck I telescope and HIRES spectrograph (Vogt

et al. 1994). Two 45-minute exposures of each star were made in sub-arcsecond seeing conditions through a 1.1-arcsec slit, giving $R = 35,000$ over a 4 pixel resolution element. A combined signal-to-noise ratio ≥ 40 per pixel, or $S/N > 80$ per resolution element, was attained after coaddition. Similar observations of the F-supergiant (A-207) were taken on August 4, 1995. Weather conditions only allowed for two exposures, one for 50 minutes and a second for 30 minutes; since this star is fainter than the A-supergiants, the overall signal-to-noise is somewhat lower, $S/N \sim 50$ per resolution element. The wavelength range spanned $4300 \text{ \AA} \leq \lambda \leq 6700 \text{ \AA}$ in 30 echelle orders, although the wavelength coverage was not complete for $\lambda > 5000 \text{ \AA}$ on the TK2048 CCD used. The FWHM of the Keck images, as measured in the CCD spectra perpendicular to the dispersion, was 0.85 arcseconds (dominated by atmospheric seeing), or 2.2 pixels after on-chip binning by $2\times$ in the spatial direction. Slit length was limited to 7.0 arcseconds on the sky to prevent overlapping orders at the short wavelength extreme. Such high quality spectra had only been possible for Galactic and Magellanic Cloud stars before.

The two-dimensional CCD echelle spectrograms were reduced at Caltech using a set of routines written for echelle data reduction (c.f., McCarthy *et al.* 1995, McCarthy & Nemec 1997) within the FIGARO package. Even though the stars are isolated and not within H II regions, the stellar HIRES spectra revealed significant broad (over 300 km s^{-1}) nebular contamination of the Balmer line profiles, easily recognizable to the sides of the stellar spectra in the two-dimensional CCD data. This nebular contamination was removed from the stellar spectra prior to extraction by fitting low-order polynomials to “sky apertures” adjacent to the stellar spectrum in the spatial direction on the slit (also discussed in McCarthy *et al.* 1995 for analysis of individual stars in M33).

Three targets (41-3712, 41-2368, & 41-3654) were selected from the low resolution survey of luminous blue stars in M31 by Humphreys, Massey & Freedman (1990). Additionally, 41-3712 and 41-3654 were confirmed as isolated, normal A-type supergiants from low resolution spectroscopy by Herrero *et al.* (1994). An additional target (A-207) was selected from Humphreys (1979) because of its location in Baade’s Field IV. [Note, that A-207 is in the western-most of three small associations identified in Plate IV of Baade & Swope (1963), and it is not the star labelled “207” in Figure 2 of Humphreys (1979), which is instead B-207]. Coordinates and UBV colors are listed in Table 1. Their estimated locations on an HRD are shown in Fig. 1. Sample spectra are shown in Figs. 2 and 3.

3. Atmospheric Analyses

The M31 A-F supergiant photospheres have been analysed using ATLAS9 (hydrostatic, line-blanketed, plane parallel) model atmospheres (Kurucz 1979, 1988). These atmospheres have been used successfully for photospheric analyses of A-F supergiants in the Galaxy and Magellanic Clouds (Venn 1995a, 1995b, 1999, Luck *et al.* 1998, Hill 1997, Hill *et al.* 1995). However, as seen in Fig. 1, the stars analysed here are more luminous than previously studied A-F supergiants (by Venn 1995a, 1999), which poses a few new challenges.

Firstly, these stars have stronger radiation fields such that departures from LTE can be expected to increase. An examination of LTE-grey, LTE-line-blanketed, NLTE-grey, and NLTE-partially-blanketed models has been carried out by Przybilla (1997). He has shown that these atmospheres are remarkably similar deep in the photosphere where the continuum forms. In fact, the largest effect in this atmospheric region is caused by neglecting line-blanketing. Thus, we have elected to use the fully line-blanketed ATLAS9 model atmospheres as the best representation of the photospheric continuum and deep line forming regions.

Secondly, the stronger radiation fields can create velocity fields and a stellar wind. 41-3654 and 41-3712 have strong stellar winds, as seen by their H α P Cygni profiles in Fig. 9 and 12 in McCarthy *et al.* (1997). The stellar wind in 41-3654 is much stronger than that in 41-3712, seen empirically by comparing the heights of the H α P Cygni emission peaks, and the fact that H β still has a P Cygni profile in 41-3654, but not 41-3712. P Cygni profiles can also be seen in some very strong Fe II lines, e.g., see Fe II 5169 in Fig 3. Only weak lines that form deep in the photosphere are used in the supergiant analyses, which are not usually sensitive to velocity fields. In the case of 41-3654, we know the velocity field affects the photosphere and can affect our analysis (discussed below), but the photosphere of 41-3712 is not affected by its wind (see McCarthy *et al.* 1997).

Thirdly, one may question whether these stars are spherically extended. Calculations of the atmospheric thicknesses (between $\tau_{5000}=2/3$ and 0.001) and the stellar radii (based on M_{bol} and effective temperature, see Venn 1995b) show that atmospheric extension is $\sim 3\%$ for three stars, 41-2368, 41-3712, and A-207. Extension for the fourth star, 41-3654, may be as large as 10%, which is a significant amount and is discussed further below.

A summary of the atmospheric parameters determined here for the stars in M31 are listed in Table 1. The methods for these determinations are discussed individually below.

3.1. M31-41-3712 & M31-41-2368 Atmospheres

Spectral features have been used to determine the model atmosphere parameters for 41-3712 and 41-2368, in particular the wings of the $H\gamma$ line profile (e.g., Fig. 4) and ionization equilibrium of Mg I/Mg II (e.g., Fig. 5). These features were rigorously examined for normal Galactic A-supergiants by Venn (1995b), and can be expected to yield reliable parameters to within $\Delta T_{\text{eff}} = \pm 200$ K, $\Delta \log g = \pm 0.1$. Both 41-3712 and 41-2368 appear to be normal A-type supergiants, thus this analysis method is appropriate for these two stars.

Examination of $H\alpha$ shows that 41-2368 has a very weak wind affecting only the core of the line, whereas 41-3712 exhibits a significant P Cygni profile indicating a substantial wind. McCarthy *et al.* (1997) have analysed the wind of 41-3712 in detail, and found a mass loss rate of $\dot{M} = 1.1 \pm 0.2 \times 10^{-6} M_{\odot}/\text{yr}$. However, their analysis has also shown that the deeper layers of the atmosphere are unaffected by the wind, which has only a mild influence on $H\beta$ and is almost negligible for $H\gamma$. Nevertheless, the blue wing of $H\gamma$ was primarily scrutinized for atmospheric parameter constraints, see Fig. 4.

NLTE corrections have been calculated for Mg I and Mg II in both stars, and included in the ionization equilibrium calculations. The corrections are negligible for the Mg II lines in both stars ($\Delta \log(\text{Mg II}/\text{H}) = \leq 0.05$), while the corrections for the $\log(\text{Mg I}/\text{H})$ abundances range from +0.02 to +0.23 dex, correlated with line strength. Lines stronger than 200 mÅ were neglected since these lines form over several atmospheric layers, including some at small optical depths. The Mg NLTE calculations use the Gigas (1988) Mg I/Mg II model atom and a system of programs first developed by W. Steenbock at Kiel University and further developed and upgraded by M. Lemke. Mg NLTE calculations in Galactic A-F supergiants have been described by Venn (1995b).

There are two ionization states of iron available in these stars as well, however equilibrium of Fe I/Fe II is not used for atmospheric parameter determinations in these stars. These stars are moderately-warm A-type supergiants where NLTE effects on Fe I lines are expected to be large, 0.2 to 0.3 dex (c.f., Boyarchuk *et al.* 1985, Gigas 1986). Fe I is overionized by the UV radiation field in these stars, but this has a negligible effect on Fe II which is the dominant ionization state. Thus, the same authors predict that NLTE effects are negligible for Fe II lines, also confirmed by more recent detailed calculations by Becker (1998).

Microturbulence (ξ) was found by examining the line abundances for Ti II, Cr II, Fe II (and Fe I for 41-2368), and requiring no relationship with equivalent width. Allowing for an uncertainty in $\Delta \xi$ of $\pm 1 \text{ km s}^{-1}$ brings the results from the different species into very good agreement.

3.2. M31-A-207 Atmosphere

A-207 is a much cooler star than 41-2368 and 41-3712, with no weak Mg I lines useful for atmospheric parameter determinations. Thus, the atmospheric parameters for A-207 were determined by comparing the results from other spectroscopic, and photometric, indicators.

UBVR colors: Firstly, the *UBVR* colors for A-207 were compared to theoretical calibrations by Bessell *et al.* (1998), after an *a priori* estimate of reddening from its spectral type. *UBV* colors are reported in Table 1. Color indices are sensitive to temperature in F-type stars, however our results for $(B - V)$, $(U - B)$, and $(V - R)$ are not in good agreement with each other. For example, from the Bessell *et al.* (1998) calibrations, $(B - V)$ implies $T_{\text{eff}}=6250$ at $\log g=0.5$, whereas $(U - B)$ suggests $T_{\text{eff}}=8250$ at $\log g=1.0$ (these are the lowest gravity models reported). Also, $(V - R)$ is degenerate with T_{eff} ranging from 5000 to 9000 K near $\log g=1.0$. The range in these color calibrations is as large as the A-F temperature range. Thus, the atmospheric parameters for A-207 were selected from spectral features.

H γ wings: The H γ profile was examined (as was done for the other stars in this paper), and yet most fits are rather poor for A-207. This is partially due to the quality of the spectrum in the bluest orders, as well as the significant metal-line blending. The best fits to H γ in A-207 are shown in Fig. 6; fits are strongly T_{eff} sensitive, but only weakly gravity sensitive.

Fe I versus χ : Another spectroscopic parameter is the Fe I line abundance versus lower excitation potential (χ). This has been used successfully as a temperature indicator for F-supergiants in the past (e.g., Luck *et al.* 1998, Luck & Lambert 1992). This proved to be the least reliable indicator for our dataset though, primarily because of the high scatter in the line abundances. Even after the spectrum was carefully scrutinized to search for potential blends and after the atomic data was carefully reviewed, the full range in the best 41 Fe I lines (out of over 200 measured features) was $\Delta\log(\text{Fe I}/\text{H}) \sim 1.0$ dex. Negligible trends in $\log(\text{Fe}/\text{H})$ vs χ were seen in the range of 6500 to 8500 K (for low gravity atmospheres), the same range found from the *UBV* colors.

Fe I versus Fe II: The average Fe I and Fe II abundances were examined for ionization equilibrium. For F-supergiants, temperature is usually selected from one of the methods above, and iron ionization equilibrium is used only for gravity (c.f., Luck *et al.* 1998, Hill 1997, Luck & Lambert 1992). Since no method above produced a well defined temperature, then Fe I/Fe II is used here to examine both temperature and gravity (as H γ was used). Throughout the elemental abundance analyses (discussed further below), strong lines are

eliminated from the line list; for A-207, a limit of $W_\lambda \leq 160 \text{ m}\text{\AA}$ was adopted. Nevertheless, the scatter in the Fe I and Fe II abundances is large, $1\sigma \sim 0.3$ and 0.2 dex, respectively. This scatter is similar to that found in other F-G supergiant analyses (e.g., Hill 1997, Luck *et al.* 1998, Luck & Lambert 1992, Russell & Bessell 1989). Finally, a locus of T_{eff} -gravity pairs that reproduce Fe ionization equilibrium was calculated for A-207.

Parameters for A-207: The final atmospheric parameters for A-207 have been selected as $T_{\text{eff}}=6700 \pm 300 \text{ K}$ and $\log g=0.2 \pm 0.2$, with $\xi=8 \pm 2 \text{ km s}^{-1}$. The loci of iron ionization equilibrium and $\text{H}\gamma$ T_{eff} -gravity pairs are shown in Fig. 7. The uncertainty in ξ in this star is larger than for the others in this paper because of the large scatter in the line abundances.

3.3. M31-41-3654 Atmosphere

Standard spectroscopic features for the analysis of an A-type supergiant have been observed in 41-3654 (e.g., $\text{H}\gamma$, Mg I, and Mg II features are observed in the spectrum, see Figs. 2 and 3), however we consider our analysis of this star only preliminary in this paper. This star has a very strong stellar wind, examined in detail by McCarthy *et al.* (1997), which is expected to impact the line forming region of the photosphere, unlike the A-F supergiants previously analysed (e.g., Venn 1995b, Luck *et al.* 1998). This will affect the pressure and temperature stratification in a model atmosphere, and it means that most of the standard assumptions in the ATLAS9 models will not apply, e.g., hydrostatic equilibrium and LTE.

In this preliminary analysis, we simply examine the $\text{H}\gamma$ profile, and Mg I/Mg II equilibrium. No standard ATLAS9 model could be generated to fit the $\text{H}\gamma$ line profile, i.e., the lowest gravities were still too large. The observed $\text{H}\gamma$ line profile forms over several layers in a stellar atmosphere, although the wings form primarily in the photosphere which is why it is usually a useful photospheric diagnostic. A stellar wind can contribute to $\text{H}\gamma$ (line filling due to wind emission), but also incoherent electron scattering can also fill the line wings (see discussion by McCarthy *et al.* 1997). Thus, $\text{H}\gamma$ has only limited use for gravity determinations in the most luminous supergiants. More specifically, ATLAS9 fails to fit the 41-3654 $\text{H}\gamma$ line profile because the radiative pressure due to the line opacity is too strong in this star (i.e., $g_{\text{rad}} > g$), thus hydrostatic equilibrium breaks down and there is an outward acceleration, i.e., a stellar wind. McCarthy *et al.* (1997) used unified model atmospheres (calculated according to Santolaya-Rey *et al.* 1997) that include spherical geometry, radiative equilibrium, and NLTE radiative transfer in the comoving frame, but not line blanketing, and they managed to fit the observed $\text{H}\gamma$ profile with $T_{\text{eff}}=8900$ and $\log g=0.9$. The unified models are ideal for a stellar winds analysis, but not for an analysis

of the stellar photosphere, e.g., since they neglect line blanketing.

Further tests with ATLAS9 showed that Mg ionization equilibrium could be attained with parameters ranging from $T_{\text{eff}}/\text{gravity} = 8500/0.8$ to $9100/1.3$ (using the NLTE corrected abundances). All of these models result in near solar Mg but significantly depleted iron-group elements, $\log(\text{Fe,Cr,Ti}/\text{H}) \sim -0.5$. The Mg and iron-group results are not significant though since an appropriate ATLAS9 model atmosphere could not be generated. The stellar wind effects (and possibly NLTE) effects on the atmospheric structure (not accounted for in ATLAS9) will affect the photospheric abundance determinations. Firstly, if the model atmosphere structure is distorted by NLTE and stellar wind effects, then this would affect the Mg ionization equilibrium since the Mg I and Mg II features form at slightly different optical depths. For example, Mg I $\lambda 5183$ has $\chi = 2.72$ eV and forms near $\log(\tau_{5000}) \sim -1$, while Mg II $\lambda 4390$ has $\chi = 10.00$ eV and forms near $\log(\tau_{5000}) \sim -0.4$. Similarly, the Ti II lines form in a similar location to Mg I whereas the Cr II and Fe II lines tend to form in deeper layers. Secondly, a simple calculation of the atmospheric extension for 41-3654 is $\sim 5\text{--}10\%$ (between $\tau_{5000} = 2/3$ and 0.001) based on the range of atmospheric parameters estimated for this star. A study of ATLAS models by Fieldus *et al.* (1990) found that 10% extension in A-supergiants could weaken moderately-strong ($\sim 100\text{ m}\text{\AA}$) Fe II lines by $\sim 10\%$. An additional important effect is the influence of incoherent electron scattering resulting from the large extension of the photosphere (discussed by McCarthy *et al.* 1997) which would weaken the lines even further. We have tried scaling our equivalent widths up by 10% and find that the abundances increase, $\Delta\log(X/\text{H}) = +0.1$ to 0.2 .

Finally, we note that the helium abundance in an A-supergiant atmosphere can also have an effect on its structure (c.f., Kudritzki 1973, Humphreys, Kudritzki & Groth 1991). Test calculations show that changing helium from 9% (ATLAS9 standard) to 20% in an A-supergiant atmosphere increases the Balmer jump and Balmer line strengths. This is because an increase in helium affects the mean molecular weight of a column of gas, which affects the opacity and pressure stratification. But also, helium is mostly neutral in A-type stars, thus reducing the number of free electrons available for Thompson scattering (the dominant opacity source at these temperatures). Unfortunately, He I lines are only observed in early A-type stars, and NLTE analysis of these lines have provided inconsistent helium abundances in the past (c.f., Husfeld 1994). Thus, determination of helium abundances in specific stars is uncertain. However, our test calculations (increasing helium from 9 to 20%) also show that the effects are essentially identical to an increase in gravity ($\Delta\log g \sim +0.2$) for 41-3712, e.g., the Balmer line profiles and the metal line abundances are *identical*. On the other hand, this is not the case for 41-3654; a change in both gravity and temperature are indicated to maintain Mg ionization equilibrium, also the derived Mg abundance itself increases. This is due to larger NLTE corrections for both species in this slightly hotter

star.

Thus, we consider our analysis of the atmospheric parameters of 41-3654 as preliminary. Significant improvement to this preliminary analysis requires model developments that are beyond the scope of this paper. We include our results in Table 1, but we do not consider this star throughout the discussion.

4. Elemental Abundances

Elemental abundances have been calculated using both spectrum syntheses and individual line width analyses. All calculations have been done using a modified and updated version of LINFOR⁷.

Equivalent widths are listed in Table 2 for the non-iron group elements (as an example). For all lines, atomic data was adopted from the literature; an attempt has been made to adopt, (1) laboratory measurements data, e.g., O’Brien *et al.* 1991 for Fe I, and (2) opacity project data, e.g., Biemont *et al.* (1991) for O I. (3) or critically examined atomic data, e.g., NIST data (c.f., <http://physics.nist.gov>). Semi-empirical values calculated by Kurucz (1988, also see <http://cfa-www.harvard.edu/amdata>) were adopted when necessary. Solar abundances are adopted from Grevesse & Sauval (1998).

Not all spectral lines observed were used in this analysis. In particular, strong lines were neglected. In most cases, strong lines include those with $W_\lambda \geq 200 \text{ m}\text{\AA}$, e.g., the line strength where the uncertainty in microturbulence ($\sim \pm 1 \text{ km s}^{-1}$) yields an change in $\log(X/H) \sim \pm 0.1$ dex. In some cases, a smaller W_λ limit was used if large deviations in the abundances were apparent after a preliminary analysis; e.g., in A-207, only Fe I lines weaker than $160 \text{ m}\text{\AA}$ were included. Weak lines help to ward off uncertainties in the model atmospheres analysis due to NLTE and spherical extension in the atmospheric structure, as well as NLTE and microturbulence effects in the line formation calculations.

Average elemental abundances for each star are listed in Table 3. One sigma errors are tabulated based only on the line-to-line scatter. All oxygen abundances are from spectrum synthesis of the 6158 \AA feature; the observed spectra and synthesis fits are shown in Fig 8. In A-207, the feature is blended with Si I, which was included in the synthesis and its abundance was allowed to vary; the oxygen results were nearly insensitive to the silicon abundances, e.g., $\Delta \log(\text{Si}/H) = \pm 0.3$ caused $\Delta \log(\text{O}/H) = \pm 0.02$. NLTE effects on the

⁷LINFOR was original developed by H. Holweger, W. Steffen, and W. Steenbock at Kiel University. Since, it has been upgraded and maintained by M. Lemke, with additional modifications by N. Przybilla.

O I 6158 feature are predicted to be small in A-supergiants, and negligible for F-supergiants. For example, a correction of $\Delta\log(\text{O}/\text{H})=-0.25$ is predicted from detailed NLTE analyses (Przybilla *et al.* 2000, also in good agreement are the earlier detailed studies by Takeda 1992 and Baschek *et al.* 1977) for the atmospheric parameters of 41-3712. The predictions reduce to $\Delta\log(\text{O}/\text{H})=-0.20$ and 0.0 for 41-2368 and A207, respectively. LTE and NLTE O I abundances are listed in Table 3.

For all three stars, synthesis of three Fe II lines was done at the same time as the oxygen spectral syntheses (i.e., absorption lines at $\lambda 6147$, $\lambda 6149$, and $\lambda 6150$). The syntheses of these Fe II lines was used to estimate rotational velocities (see Table 1), and the iron abundance results were included in the average Fe II abundances in Table 3.

Several lines of s- and r-process elements have been observed (see examples in Figs. 2 and 3) and analysed in two stars. Note that only one to four lines per species have been analysed (see Tables 2 and 3), making these results somewhat uncertain, e.g., unknown blends, quality of the atomic data, unrecognized NLTE effects. Several additional lines were observed in A-207, however their line strengths are well over 200 mÅ and are not considered reliable abundance indicators. This is especially true considering their low excitation potentials, indicating line formation at optical depths above the photosphere. With respect to NLTE effects on the s- and r-process line formation, Lyubimkov & Boyarchuk (1982) found that Ba abundances measured from resonance lines are 0.2 to 0.4 dex less than those from subordinate lines in Canopus (an F-type supergiant). In this analysis, barium is measured from two resonance lines and one subordinate line, however the abundances are in very good agreement, $\Delta\log(\text{Ba}/\text{H})=0.05$ dex only. Thus, either the NLTE corrections are smaller than predicted for the resonance lines, or both resonance and subordinate lines are affected uniformly. NLTE effects on other s- and r-process elements are not currently available.

To ascertain the reliability of these heavy element abundances, we have examined the published abundances in Galactic F-supergiants by Luck *et al.* (1998). Luck *et al.* analysed up to 11 species of s- and r-process elements in 11 F-G supergiants, including all of the species in this paper. They measured one to 18 lines per element. The typical *range* in the Y II, Zr II, Ce II, and Nd II abundances in any one star examined by Luck *et al.* is ± 0.1 dex. This strongly suggests that the s- and r-process abundances can be reliably determined in cool supergiants. In this paper, we find the weighted average s- and r-process abundances to be $[\text{s+r}/\text{H}]=+0.18 \pm 0.15$ and $+0.22 \pm 0.02$ for A-207 and 41-2368, respectively.

Abundance uncertainties due to $\Delta T_{\text{eff}}=+200$ K, $\Delta\log g=-0.1$ are shown for the two A-stars in Table 4. Uncertainties due to microturbulence ($\Delta\xi=\pm 1$ km s⁻¹) are not listed since they are very small (~ 0.02 to 0.05 dex) in this weak line analysis. For A-207,

abundance uncertainties due $\Delta T_{\text{eff}} = +300 \text{ K}$, $\Delta \log g = -0.2$ and $\Delta \xi = -2 \text{ km s}^{-1}$ are shown in Table 4.

5. Discussion

Stellar abundance calculations in M31 can be used to address several questions:

(1) Do the stellar oxygen abundances show the same abundance gradient in M31 as the nebular oxygen abundances?

(2) What are the abundances of other elements in M31? Do these elements also show radial gradients? What can differences in the element ratio gradients tell us about the chemical evolution of M31?

(3) How do the analyses of A-F supergiants in M31 improve the Cepheid distance determinations through more accurate metallicity and reddening determinations?

Each of these will be addressed separately in the following subsections. We stress that three stars are insufficient to answer any of these questions at this time; in this discussion, we shall simply show how stellar abundances in M31 can be used, particularly if we can increase the sample size.

5.1. The Oxygen Abundance Gradient in M31

Oxygen and nitrogen abundances in M31, as inferred from the analysis of H II regions have been investigated by Blair *et al.* (1982 = BKC82) and Dennefeld & Kunth (1981). Their results are in good agreement with each other, and in Fig. 9 we plot their nebular oxygen abundances as a function of M31 galactocentric distance (R_{M31}). We also show a least squares fit to these data which implies a radial abundance gradient of $-0.029 \text{ dex kpc}^{-1}$ (intercept value $12 + \log(\text{O}/\text{H}) = 9.12 \text{ dex}$, same as BKC82).

Uncertainties in the slope are significant; the oxygen abundance drops by about a factor of 4, and yet the uncertainty in each oxygen abundance is about a factor of 2, and the range in the data at a given R_{M31} is about a factor of 2 to 3. Thus, the oxygen radial gradient is rather uncertain, $-0.029 \pm 0.023 \text{ dex kpc}^{-1}$. Most of the uncertainties (per nebula, as well as the range from various nebulae at the same R_{M31}) come from uncertainties in the R_{23} empirical calibration(s) used. BKC82 based their nebular analysis on the calibrations by Pagel *et al.* (1979), although their H II regions had a larger range in metallicity and lower excitation than those used by Pagel *et al.* for the calibration. Vila-Costas & Edmunds

(1992) obtained a slightly higher gradient ($-0.043 \text{ dex kpc}^{-1}$) from a recalculation of O/H from the published line intensities using updated R_{23} calibrations by Edmunds & Pagel (1984) and supplementing the high and low metallicity regions with calibrations by Edmunds (1989) and Skillman (1989), respectively. Similarly, Zaritsky, Kennicutt & Huchra (1994 = ZKH94) found a more shallow gradient, $-0.018 \pm 0.006 \text{ dex kpc}^{-1}$, by computing mean oxygen abundances from three different calibrations (Edmunds & Pagel 1984, Dopita & Evans 1986, and McCall *et al.* 1985). Uncertainties in the oxygen abundances are estimated as $\pm 0.2 \text{ dex}$ from the Pagel *et al.* (1979) R_{23} calibration (Pagel *et al.* 1980), yet ZKH94 found that the dispersion between the three methods they examined dominated their oxygen uncertainties.

In Fig. 9 we show the positions and (NLTE) oxygen abundances of the three A-F supergiants analysed here. The stellar positions were calculated adopting the same parameters for M31 as from Blair *et al.* (1982) for comparison purposes (i.e., 690 kpc distance to M31, 37.5° position angle for the major axis, 77.5° inclination). The stellar abundances are consistent with the nebular picture, i.e., the stellar oxygen abundances lie within the range of nebular results, and yet there are three striking points to the stellar abundances. Firstly, the stellar abundance uncertainties are noticeably smaller than the full range in the nebular abundances; this is probably due to uncertainties in the application of the R_{23} calibrations, since individual nebular abundances should have similar uncertainties to the stellar abundances. Secondly, the two stars near 10 kpc yield very similar oxygen abundances ($\log(\text{O}/\text{H}) \sim 8.75$), and these abundances are in excellent agreement with the mean nebular abundance from BKC82 ($\log(\text{O}/\text{H}) \sim 8.7$) at this R_{M31} distance. Thirdly, the star near 20 kpc has an abundance in excellent agreement with the mean nebular abundance from ZKH94 ($\log(\text{O}/\text{H}) \sim 8.8$), but this abundance is also similar to those near 10 kpc. This is interesting because the stellar abundances suggest that there is no radial gradient between 10 and 20 kpc.

Stellar and nebular oxygen abundances are usually in very good agreement. For example, Cunha & Lambert (1992) found very good agreement between the Orion nebular oxygen abundances and B-star abundances. Smartt & Rolleston (1997) determined oxygen in B-stars in the Galaxy and found the same radial gradient as from nebulae. Venn (1999) found that B-stars, A-F supergiants, and nebulae all yield the same oxygen abundances in the SMC. McCarthy *et al.* (1995) and Monteverde *et al.* (1997) find oxygen from B-A supergiants in M33 that are in good agreement with the oxygen gradient from nebular studies in that galaxy. Thus, we return to the third point above to further discuss the nature of the oxygen gradient in M31 beyond $\sim 10 \text{ kpc}$.

To examine the gradient beyond 10 kpc, we need to ascertain the reliability of the

stellar and nebular abundances. Firstly, are the stellar abundances sufficiently reliable to examine the oxygen gradient? We suggest that they are. Analysis of A-F supergiants in the Galaxy and Magellanic Clouds have found oxygen abundances in good agreement with nebular results from similar model atmosphere analyses (Venn 1999, Luck *et al.* 1998, Hill 1997, Hill *et al.* 1995, Luck & Lambert 1992, Russell & Bessell 1989). Furthermore, the O I feature analysed here in all three stars is simply not very sensitive to the standard uncertainties in this analysis (e.g., T_{eff} , gravity, ξ , see Table 4, also the NLTE corrections are quite consistent between various detailed NLTE analyses and the corrections are modest). Secondly, how significant is the gradient reported from the nebular abundances? For example, we notice that the nebular abundances show a large range in oxygen at any given R_{M31} . This is interesting since there has been some discussion on the shape of abundance gradients in spiral galaxies. For example, the question “Do radial gradients flatten out?” has been posed through observational and theoretical studies (e.g., Mollá *et al.* 1996, Zaritsky 1992, Vilchez *et al.* 1988). Zaritsky (1992) predicts that the radial abundance profile of a spiral galaxy changes slope where the rotation curve levels off, a situation that arises from star-formation in a viscous disk model. In the case of M31, one would expect this break to occur at $R_{\text{M31}} = 6$ to 8 kpc (rotation curves for M31 by Rubin & Ford 1970, Roberts & Whitehurst 1975). This is not *clearly* seen in the nebular data, although neglecting the innermost H II (with $R_{\text{M31}} < 10$ kpc) would result in a very flat gradient, possibly suggesting a two-component gradient as predicted. The mean value of oxygen in the outer disk would then be $12 + \log(\text{O}/\text{H}) \sim 8.7$, which is in excellent agreement with the mean of the three stellar abundances presented here, $\log(\text{O}/\text{H}) \sim 8.75$.

Finally, we note that Brewer *et al.* (1995) also suggested that the abundance gradient in M31 flattens out in the outer disk. They deduce abundances from the ratio of C-type (C-poor) to M-type (C-rich) AGB stars, and included a field at $R_{\text{M31}} = 32$ kpc which had a similar (though highly uncertain) result to their fields near 10 kpc.

There are many isolated A-F supergiants throughout the disk of M31, although most tend to be near a ring of OB associations located near $R_{\text{M31}} \sim 10$ kpc (see van den Bergh 1964). Observing more stars (≥ 15), especially some at $R_{\text{M31}} < 10$ kpc and > 20 kpc, is desirable. Given the small uncertainties in the oxygen abundances from these stars, they are valuable in addressing the question of the nature of the oxygen abundance gradient in M31.

5.2. Element Ratios and the Chemical Evolution of M31

A high resolution analysis of A-F supergiants allows us to determine the abundances of many elements beyond oxygen. Among the three stars analysed in this paper, we have also found the abundances for several other α -elements, as well as iron-group and heavier elements.

We have plotted the abundances of other elements versus R_{M31} in Fig. 10. To reduce random errors, we have plotted a weighted mean of all the α (except O), iron-group, and s- and r-process elements per star. There is the suggestion of an abundance gradient in all of these elements, in agreement with the *nebular* oxygen gradient. However, the data are also consistent with no gradients beyond 10 kpc, as predicted in the viscous disk model. It is worth noting here that NLTE effects have been neglected for all elements, other than O and Mg. This may have an effect on the $[\alpha/H]$ and $[s+r/H]$ plots, but should not affect the $[Fe/H]$ plot. Iron-group abundances are calculated from the dominate ionization species in all three stars, where NLTE effects are predicted to be quite small (see NLTE comments above for iron).

A potentially more interesting and valuable constraint comes from element ratios, e.g., $[O/Fe]$, particularly versus R_{M31} as shown in Fig. 11. Element ratios are useful because they are very sensitive to assumptions made in chemical evolution models (e.g., star formation rates, the IMF, stellar yields, etc., see the recent review by Henry & Worthy 1999 and the references cited therein). The proportional buildup of elements relative to one another depend on differences in their nucleosynthetic origins, e.g., O/Fe depends on the star formation history because O is produced primarily through the evolution of massive stars, whereas iron is ejected from all supernova events. α -elements have similar nucleosynthetic sources as oxygen, and yet the yields may vary, which affects the observed ratios, e.g., O/Fe versus Mg/Fe. Meanwhile, the s- and r-process elements come from a very different source, intermediate-mass stars undergoing thermal pulsing on the AGB, and therefore are sensitive to the IMF.

In Fig. 11, $[O/Fe]$, $[s+r/Fe]$, and possibly $[\alpha/Fe]$ (note that this mean α ratio does not include oxygen), appear to increase in the outer disk of M31. We note that these increases are strongly dependent on the iron-group abundance in the outer most star, A-207; the uncertainty in the iron-group abundances for this star is larger than usual (as discussed above, and noted by the errorbar); however, we also believe that we have minimized potential systematic errors in the analysis of this star, and that the data point is accurate within its errorbar. With so few stars, the gradients (or lack of gradients) in these plots are not statistically significant. However, a gradient in $[O/Fe]$ is intriguing because, if confirmed by further work, then higher O/Fe in the outer disk of M31 could suggest, e.g., a recent

burst of star formation or a change in the IMF. Clearly, more stars need to be observed to discuss this further.

Finally, we note that the oxygen and iron abundance uncertainties are quite similar in the early A-type supergiants when oxygen is determined from the O I $\lambda 6156$ feature and iron from Fe II lines (see Table 4). This means that systematic errors in the model atmospheres analysis are reduced when the O/Fe *ratio* is examined. This is not true for the cooler F-supergiants though, thus the most accurate investigation of [O/Fe] in M31 would concentrate on early- to mid-A supergiants only. Unfortunately, securing enough of these targets, over a narrow range in temperature, and yet a large range in galactocentric radii, could be difficult.

5.3. Cepheid Metallicities & Reddenings

A-F supergiant analyses are relevant to Cepheid distance determinations. These stars have similar young ages and intermediate-masses, and therefore should have very similar compositions and galactic (thin disk) locations to those of the Cepheids. A-F supergiant atmospheric analyses provide direct elemental abundances, as well as local reddening estimates.

5.3.1. Metallicities

The true effects of metallicity on the Cepheid PL relationship remain uncertain, but are expected to affect Cepheid distances at less than the 10% level in M31 and Hubble Key Project galaxies (see discussion by Kennicutt *et al.* 1998). Metallicity is important because it increases line blanketing, which affects the Cepheid color calibrations and their mean magnitudes e.g., brighter mean magnitudes and redder colors are predicted at higher abundances.

In Kennicutt *et al.* ’s (1998) discussion of the metallicity effect, they examined Cepheids in two fields in M101, a spiral galaxy with a steep oxygen abundance gradient, and reviewed the results from studies in other galaxies. The conclusions from all of the studies suggests an uncertainty in the distance modulus (μ) of $\Delta\mu \sim -0.25 \pm 0.2 \text{ mag dex}^{-1}$ in *VI* luminosity. They conclude that this relationship between μ and metallicity is consistent with theory ($\Delta\mu \sim -0.1 \text{ mag dex}^{-1}$ in *VI* luminosity), but they also note that it is consistent with no dependence at all.

In M31, Freedman & Madore (1990, FM90) examined the Cepheid distance

determinations from *BVRI* photometry in Baade Fields I, III, and IV (Baade & Swope 1963). They adopt galactocentric radii for these fields of ~ 3 , 10 and 20 kpc, with metallicities of 0.2, 0.0 and -0.5 dex, respectively, from nebular oxygen analyses by Blair *et al.* (1982). FM90 reported $\Delta\mu = -0.32 \pm 0.21$ mag dex $^{-1}$, and concluded no significant metallicity dependence. Kennicutt *et al.* (1998) reanalysed the FM90 data by recalculating the abundance gradient in M31 (see discussion above), and found a much stronger metallicity dependence of $\Delta\mu = -0.94 \pm 0.78$ mag dex $^{-1}$. This slope would be significant if the uncertainty were smaller; as is, the result is inconclusive. Additionally, this neglects the question of the shape of the abundance gradient in M31 (discussed above), which may show no significant range in metallicity at all beyond ~ 10 kpc.

With respect to our A-F supergiants, we note that the standard assumption is that Cepheid iron-group abundances (metallicity) will scale as the nebular oxygen abundances. Clearly, this neglects potential effects due to the chemical evolution of the galaxy, i.e., iron and oxygen have different nucleosynthetic sites and thus timescales for formation and distribution in a galaxy. In the LMC and SMC, this is not a problem since analyses of A-K supergiants have found that the O/Fe ratios are the same as Galactic A-K supergiants (Venn 1999, Hill 1997, Luck *et al.* 1998, Hill *et al.* 1995, Luck & Lambert 1992, Russell & Bessell 1989). However, this may not be true in M31. The preliminary work in this paper suggests that the Fe gradient is similar to the reported O *nebular* gradient, although both the nebular and stellar data could be consistent with no gradients beyond 10 kpc. Determination of the actual iron abundances in the disk of M31 would allow for a proper test of metallicity effects on the Cepheid PL relationship.

5.3.2. Reddening

One of the more significant sources of uncertainty in Cepheid distance calculations today is simply the reddening estimate; in particular how changes in metallicity can affect Cepheid colors and cause incorrect reddening estimates derived from multi-wavelength Cepheid photometry. A-F supergiants can play a valuable role since these stars have similar thin-disk locations as Cepheids. Local reddening estimates from A-F supergiants should be similar for nearby Cepheids, assuming that the mean reddening does not vary too widely within small regions of M31; or, at least, they can provide a check on the Cepheid values. Also, local stellar values of reddening should be more accurate than using global reddening laws.

In this paper, we deduce the reddening to our targets using the photometry listed in Table 1 and the spectral type-to- $(B - V)_0$ calibration by Fitzgerald (1970, =F70),

and the UBV colors deduced from the adopted ATLAS9 model atmospheres (program UBVBUSER⁸). Uncertainties in the F70 values noted below are estimated from the calibration scale itself (thus, internal). Also, we note that the minimum amount of foreground reddening to M31 has been pegged at $E(B - V)=0.08$ by Burstein & Heiles (1984), and more recently at $E(B - V)=0.06$ by Schlegel *et al.* (1998).

For 41-3712, the A3Ia spectral type is in good agreement with our atmospheric parameters, and implies $(B - V)_o=0.06 \pm 0.04$ from F70 and $(B - V)_o=0.09$ from the ATLAS9 model. Thus, we find $E(B - V)=0.03$ to 0.06 ± 0.04 , in agreement with the foreground estimates. This star is in close proximity to a Cepheid variable, V7184 in M31B, found by Kaluzny *et al.* (1998); their separation is $44''$ on the sky, or 0.8 kpc in the disk. For field M31B, Kaluzny *et al.* have adopted a mean reddening of $E(B - V)=0.20$ [this high reddening value is in agreement with the old Berkhuijsen *et al.* (1988) photometry, but our lower value uses the Magnier *et al.* (1992, 1993) CCD photometry]. This difference would produce an uncertainty of $\Delta\mu \sim +0.46$ (using $R_v=3.1$) in the BV luminosity.

For 41-2368, the A8Ia spectral type agrees well with our atmospheric parameters, and implies $(B - V)_o=0.14 \pm 0.02$ from F70 and $(B - V)_o=0.12$ from the ATLAS9 model. These calibrations imply $E(B - V)=0.10$ to 0.12 ± 0.08 . This star is in close proximity to Cepheid #75 from Magnier *et al.* (1997); their separation is $29''$ on the sky, or 0.4 kpc in the disk. We could not find a distance determination or reddening estimate for this star for a comparison.

For A-207 in Field IV, the F5Ia spectral type is in good agreement with our atmospheric parameters, and implies $(B - V)_o=+0.26 \pm 0.11$ from F70 and $(B - V)_o=+0.27$ from the ATLAS9 model. Thus, $E(B - V)=+0.17 \pm 0.09$ [this value is slightly higher than those found from previous studies, e.g., Baade & Swope (1963) adopted $E(B - V)=0.16 \pm 0.03$, and van den Bergh (1964) reported $E(B - V)=0.06 \pm 0.03$ to the association OB 184 in Field IV]. Freedman & Madore (1990) found $E(B - V)=0.0$ to Field IV in M31 from their $BVRI$ Cepheid photometry, but this is relative to LMC Cepheids for which they adopted a mean reddening of $E(B - V)=0.1$. Our higher reddening value implies $\Delta\mu = -0.22$ in BV luminosity (using $R_v=3.1$) for their Field IV results, and a trivial correction to their results would imply distances to Cepheids in Fields I, II, and IV that are in excellent agreement (24.33 ± 0.12 , 24.41 ± 0.09 , and now 24.36 ± 0.12 , respectively). This result is intriguing; it may suggest no significant metallicity dependence on Cepheid distances, assuming the reddening to A-207 actually does reflect that to the Cepheids in Field IV better. On the other hand, since our stellar abundances indicate no significant metallicity gradient in M31

⁸Program available from R. L. Kurucz at <http://cfaku5.harvard.edu/programs.html>

beyond 10 kpc, then perhaps metallicity effects simply cannot be tested adequately in M31.

Thus, our examination of reddening estimates in the areas sampled by our A-F supergiants might suggest some changes in Cepheid distances, ranging from $\Delta\mu \sim -0.2$ to $+0.4$, which are significant amounts.

6. Conclusions and Future Work

In this paper, we have presented new abundances for three stars in M31, and discussed these results in the context of the radial gradient in oxygen observed from nebulae. The stellar oxygen abundances are in excellent agreement with the nebular results, and yet they are more consistent with no radial gradient in oxygen (between ~ 10 and 20 kpc). This leads to questions on the exact form of the gradient, e.g., does the gradient flatten out? And/or, what is the dispersion in abundances at a given galactocentric distance? We suggest that the A-F supergiants in M31 are ideal probes to further address these questions since the uncertainties in their oxygen abundances are small, and there are plenty of these stars in the disk of M31. Observations of ≥ 15 stars, especially some at $R_{\text{M31}} < 10$ kpc and > 20 kpc, is desirable.

We have shown that many new elemental abundances in M31 can be determined from stellar abundance analyses, e.g., present-day iron abundances. The iron abundances presented here may exhibit a gradient similar to the *nebular* oxygen gradient, but we cannot discuss this in detail with observations of only three stars. The constancy of a gradient between different elements can be valuable information for chemical evolution modelling of M31. Knowing the iron abundances in the disk of M31 could also be valuable for Cepheid distance calibrations, particularly for observational tests of metallicity effects on the Cepheid PL relationship.

Finally, A-F supergiant analyses are useful as reddening indicators, which may be valuable for accurate Cepheid distance determinations. The three stars presented here are located near Cepheid variables in M31. Those Cepheids have been used to calculate distances based on global reddening laws or direct Cepheid *BVRI* photometry estimates. We find differences in the distance modulus of $\Delta\mu = -0.2$ to $+0.4$ in the *BV* luminosity for the few Cepheids examined here.

Thus, detailed stellar atmosphere analyses are now possible for individual stars in M31 and other Local Group galaxies. Stars serve as ideal probes of their environment, and can yield valuable constraints for chemical evolution models.

KAV would like to thank Macalester College and the Luce Foundation for a Clare Boothe Luce professorship award. Also, many thanks to Evan Skillman and Rob Kennicutt for helpful discussions and comments on the manuscript. JKM would like to thank the staff of the W. M. Keck Observatory, in particular observing assistant Joel Aycock, for efforts on the summit in support of these HIRES observations.

REFERENCES

- Baade, W., Swope, H.H., 1963, AJ, 68, 435
- Barlow, M.J., Cohen, M., 1977, ApJ, 213, 737
- Baschek, B., Scholz, M., Sedlmayr, E., 1977, A&A, 55, 375
- Becker, S.R., 1998, in *Boulder-Munich Workshop II: Properties of Hot Luminous Stars*, ASP Conf. Series, Vol. 131, 135
- Berkhuijsen, E.M., Humphreys, R.M, Ghigo, F.D., Zomach, W., 1988, A&A Supp., 76, 65
- Biemont, E., Hibbert, A., Godefroid, M., Vaeck, N., Fawcett, B.C., 1991, ApJ, 375, 818
- Blair, W.P., Kirshner, R.P., Chevalier, R.A., 1981, ApJ, 247, 879
- Blair, W.P., Kirshner, R.P., Chevalier, R.A., 1982, ApJ, 254, 50 (=BKC82)
- Boyarchuk, A.A., Lyubimkov, L.S., Sakhbullin, N.A., 1985, Astrophysics, 22, 203
- Brewer, J.P., Richer, H.B., Crabtree, D.R., 1995, AJ, 109, 2480
- Burstein, D., Heiles, C., 1984, ApJS, 54, 33
- Bessell, M.S., Castelli, F., Plez, B., 1998, A&A, 333, 231
- Cunha, K., Lambert, D.L., 1994, ApJ, 426, 170
- Dennefeld, M., Kunth, D., 1981, AJ, 86, 989
- Dopita, M.A., Evans, I.N., 1986., ApJ, 307, 431
- Edmunds, M.G., Pagel, B.E.J., 1984, MNRAS, 211, 507
- Edmunds, M.G., 1989, in *Evolutionary Phenomena in Galaxies*, ed.s J.E. Beckman & B.E.J. Pagel (Cambridge: Cambridge University Press), 346

- Fieldus M.S., Lester J.B., Rogers C., 1990, A&A, 230, 371
- Fitzgerald, M.P., 1970, A&A, 4, 234
- Freedman, W.L., 1985, in IAU Coll. 82, Cepheids: Theory and Observations, ed. B.F. Madore (Cambridge: Cambridge University Press), 225
- Freedman, W.L., Wilson, C.D., Madore, B.F., 1991, ApJ, 372, 455
- Freedman, W.L., Madore, B.F., 1990, ApJ, 365, 186 (=FM90)
- Gigas, D., 1986, A&A, 165, 170
- Gigas, D., 1988, A&A, 192, 264
- Grevesse, N., Sauval, A.J., 1998, Sp. Sci. Rev., 85, 161
- Hannaford, P., Lowe, R.M., Grevesse, N., Biemont, E., Whaling, W., 1982, ApJ, 261, 736
- Henry, R.B.C., Worthey, G., 1999, PASP, 762, 919
- Herrero, A., Lennon, D.J., Vilchez, J.M., Kudritzki, R.P., Humphreys, R.H., 1994, A&A, 287, 885
- Hill V., 1997, A&A, 324, 435
- Hill V., Andrievsky S., Spite M., 1995, A&A, 293, 347
- Humphreys, R.M., 1979, ApJ, 234, 854
- Humphreys, R.M., Kudritzki, R.P., Groth, H., 1991, A&A, 245, 593
- Humphreys, R.M., Massey, P., Freedman, W.L., 1990, AJ, 99, 84
- Husfeld, D., 1993, Universität München, *Habilitationsschrift*
- Jacoby, G.H., Ciardullo, R., 1999, ApJ, 515, 169
- Jacoby, G.H., Ford, H.C., 1986, ApJ, 304, 490
- Kaluzny, J., Stanek, K.Z., Krockenberger, M., Sasselov, D.D., Tonry, J.L., Mateo, M., 1998, AJ, 115, 1894
- Kennicutt, R.C., *et al.* 1998, ApJ, 498, 181
- Kennicutt, R.C., Freedman W.L., Mould J.R., 1995, AJ, 110, 1476

- Kochanuk, C.S., 1997, *ApJ*, 491, 13
- Kudritzki, R.P., 1973, *A&A*, 28, 103
- Kurucz, R.L., 1988, in *Transactions of the IAU*, Vol. XXB, M. McNally, Kluwer, Dordrecht, 168
- Kurucz, R., 1979, *ApJS*, 40, 1
- Kurucz, R.L., Peytremann, E., 1975, *SAO Special Report* 362
- Luck, R.E., Moffett, T.J., Barnes, T.G., Gieren, W.P., 1998, *AJ*, 115, 605
- Luck, R.E., Lambert, D.L., 1992, *ApJS*, 79, 303
- Lyubimkov, L.S., Boyarchuk, A.A., 1982, *Astrophysics*, 18, 596
- Magnier, E.A., Lewin, W.H.G., van Paradijs, J., Hasinger, G., Jain, A., Pietsch, W., Trümper, J., 1992, *A&A Supp.*, 96, 379
- Magnier, E.A., Lewin, W.H.G., van Paradijs, J., Hasinger, G., Pietsch, W., Trümper, J., 1993, *A&A*, 272, 695
- Magnier, E.A., Augusteijn, T., Prins, S., van Paradijs, J., Lewin W.H.G., 1997, *A&A Supp.*, 126, 401
- McCall, M.L., Rybski, P.M., Shields, G.A., 1985, *ApJS*, 57, 1
- McCarthy, J.K., Nemec, J.M., 1997, *ApJ*, 482, 203
- McCarthy, J.K., Lennon, D.J., Venn, K.A., Kudritzki, R.P., Puls, J., Najarro, F., 1995, *ApJ*, 455, 135
- Meggers, W.F., Corliss, C.H., Scribner, B.F., 1975, *NBS Monograph* 145
- Monteverde, M.I., Herrero, A., Lennon, D.J., Kudritzki, R.P., 1997, *ApJ*, 474, 107
- O'Brian, T.R., Wickliffe, M.E., Lawler, J.E., Whaling, W., Brault, J.W., 1991, *J. Opt. Soc. Am.*, B8, 1185
- Pagel, B.E.J., Edmunds, M.G., Blackwell, D.E., Chun, M.S., Smith, G., 1979, *MNRAS*, 184, 569
- Pagel, B.E.J., Edmunds, M.G., Smith, G., 1980, *MNRAS*, 193, 219

- Przybilla, N., Butler, K., Becker, S.R., Kudritzki, R.P., Venn, K.A., 2000, A&A, submitted
- Przybilla, N., 1997, Diplomarbeit, Ludwig Maximilians Universität, München
- Roberts, M.S., Whitehurst, R.N., 1975, ApJ, 201, 327
- Rubin, V.C., Ford, W.K., 1970, ApJ, 159, 379
- Russell, S.C., Bessell, M.S., 1989, ApJS, 70, 865
- Santolaya-Rey, A.E., Puls, J., Herrero, A., 1997, A&A, 323, 488.
- Schaller, G., Schaerer, D., Meynet, G., Maeder, A., 1992, A&A Supp., 96, 269
- Schlegel, D.J., Finkbeiner, D.P., Davis, M., 1998, ApJ, 500, 525
- Skillman, E.D., 1989, ApJ, 347, 883
- Smartt, S.J., Rolleston, W.R.J., 1997, ApJ, 481, 47
- Takeda, Y., 1992, PASJ, 44, 309
- van den Bergh, S., 1964, AJ, 69, 610
- Venn, K.A., 1995a, ApJ, 449, 839
- Venn, K.A., 1995b, ApJS, 99, 659
- Venn, K.A., 1999, ApJ, 518, 405
- Vila-Costa, M.B., Edmunds, M.G., 1992, MNRAS, 259, 121
- Vilchez, J.M., Pagel, B.E.J., Díaz, A.I., Terlevich, E., Edmunds, M.G., 1988, MNRAS, 235, 633
- Vogt, S. *et al.* , 1994, SPIE, 2198, 362
- Welch, D.L, McAlary, C.W., McLaren, R.A., Madore, B.F., 1986, ApJ, 305, 583
- Zaritsky, D., 1992, ApJ, 390, L73
- Zaritsky, D., Kennicutt, R.C., Huchra, J.P., 1994, ApJ, 420, 87 (=ZKH84)

Table 1. Atmospheric Parameters for four M31 A-type Supergiants

Star	A-207	41-3712	41-2368	41-3654
α (J2000) ^a	00 37 45.30	00 45 10.36	00 44 16.56	00 45 07.49
δ (J2000) ^a	+39 58 23.1	+41 36 53.6	+41 20 59.7	+41 37 36.5
V ^b	17.05 \pm 0.02	16.19	16.25	16.47
$(B - V)$ ^b	+0.44 \pm 0.03	+0.29	-0.15	+0.29
$(U - B)$ ^b	-0.04 \pm 0.05	-0.89	-0.63	-0.70
$(V - R)$ ^b	+0.50 \pm 0.04	+0.90	+0.99	+0.93
Sp. Ty. ^b	F5 Ia	A3 Ia	A8 Ia	A2 Ia
Magnier #	...	364858	274169	369379
V ^c	...	16.506 \pm 0.021	16.840 \pm 0.095	16.335 \pm0.014
$(B - V)$ ^c	...	0.120 \pm 0.023	0.242 \pm 0.105	0.175 \pm0.021
$(V - R)$ ^c	...	0.200 \pm 0.022	0.210 \pm 0.106	0.222 \pm0.015
T_{eff} (K)	6700 \pm 300	8400 \pm 200	8000 \pm 200	9000 \pm500
$\log g$	0.2 \pm 0.2	0.9 \pm 0.1	0.75 \pm 0.1	1.0 \pm0.3
ξ (km s ⁻¹)	8 \pm 2	8 \pm 1	8 \pm 1	10 \pm5
$v \sin i$ (km s ⁻¹)	20 \pm 5	30 \pm 5	30 \pm 5	30 \pm5
$E(B - V)$	+0.17 \pm 0.09	0.05 \pm 0.04	0.11 \pm 0.08	...
R_{M31} (kpc)	19.5	10.5	10.1	9.9

^aCoordinates from the Simbad database.

^bColors and spectral types from Berkhuijsen *et al.* (1988), except for A207 where the colors are the averaged values from Humphreys (1979). Berkhuijsen *et al.* report uncertainties in V of ± 0.2 and in colors of ± 0.3 to 0.4.

^cColors from the Magnier catalogue (Magnier *et al.* 1992, 1993). This photometry is preferred for the analyses and reddening estimates of 41-3712 and 41-2368.

Table 2. Line Strengths and Atomic Data of Non-Iron-Group Elements

Elem	RMT	λ (Å)	χ (eV)	log gf	REF [†]	A-207	41-2368	41-3712
600	6	4770.00	7.48	-2.33	op	48
600	6	4771.72	7.49	-1.76	op	158
600	22	6587.75	8.54	-1.02	op	110
800 ^a	10	6155.99	10.74	-0.67	op
800 ^a	10	6156.78	10.74	-0.45	op
800	10	6158.19	10.74	-0.31	op	...	85	85
1200	11	4702.98	4.35	-0.37	wmC	...	59	...
1200	2	5167.33	2.71	-0.86	wmB	...	174	...
1200	2	5172.70	2.71	-0.38	wmB	...	233	122
1200	2	5183.62	2.72	-0.16	wmB	...	275	150
1200	9	5528.42	4.34	-0.34	wmC	...	38	...
1201	10	4390.72	10.00	-0.53	wsmD	...	191	109
1201	9	4433.99	10.00	-0.90	wsmC	...	59	52
1400	...	4818.10	4.95	-1.57	wmD	38
1400	16	5948.55	5.08	-1.23	wmD	82
1400 ^a	29	6155.22	5.62	-0.40	kp
1401	5	5041.03	10.07	0.17	wmD	...	130	167
1401	4	5957.56	10.07	-0.35	wmD	...	92	...
2000	4	4455.89	1.90	-0.54	wmC	108
2000	35	4878.13	2.71	-0.33	wmC	128
2000	21	5581.98	2.52	-0.71	wmD	66
2000	21	5590.13	2.52	-0.71	wmD	27
2000	47	5857.46	2.93	0.23	wsmD	119
2000	18	6462.57	2.52	0.31	wmD	125
2000	18	6499.65	2.52	-0.59	wmD	54
2001	14	5307.30	7.53	-0.90	wsmD	94
2001	20	5339.19	8.44	-0.05	k88	...	68	51
3901	22	4786.58	1.03	-1.29	hl	144
3901	20	5087.42	1.08	-0.17	hl	...	47	...
3901	20	5119.11	0.99	-1.36	hl	132
3901	20	5205.73	1.03	-0.34	hl	...	61	...
3901	27	5480.73	1.72	-0.99	hl	134
3901	34	5728.89	1.84	-1.13	hl	55
5601	1	4554.04	0.00	0.16	wmA	...	150	...
5601	1	4934.10	0.00	-0.16	wmB	...	95	...
5601	2	6496.90	0.60	-0.38	wmC	...	25	...
5801	57	4486.91	0.29	-0.01	mc	103
5801	6	4593.94	0.69	0.26	mc	...	40	...
6001	50	4462.99	0.55	-0.07	wmD	44
6001	75	5130.60	1.30	0.10	wmD	89
6001	75	5293.17	0.82	-0.15	wmD	118

Table 2—Continued

Elem	RMT	λ (Å)	χ (eV)	log gf	REF [†]	A-207	41-2368	41-3712
------	-----	---------------	-------------	--------	------------------	-------	---------	---------

[†]Reference Key: wm = Wiese & Martin 1980, op = Hibbert *et al.* 1991 (O), Hibbert *et al.* 1993 (C), wsm = Wiese, Smith, & Miles 1969, hl = Hannaford *et al.* 1982, mc = Meggers *et al.* 1975, kp = Kurucz & Peytremann 1975, k88 = Kurucz 1988. Capitol letters denote estimated accuracy.

^aThese lines have been used for spectrum syntheses so that only their atomic data are reported here.

Table 3. Elemental Abundances in four M31 A-type Supergiants

Elem	Sun	Gal AI	A-207	41-3712	41-2368
C I	8.52	8.35 \pm 0.21	8.26 \pm 0.05 (3)
O I ^a	8.83	8.77 \pm 0.12	8.8 \pm 0.1 (S)	9.0 \pm 0.1 (S)	8.9 \pm 0.1 (S)
O I ^{a,b}			8.8 \pm 0.1 (S)	8.75 \pm 0.1 (S)	8.7 \pm 0.1 (S)
Mg I	7.58	7.48 \pm 0.17	...	7.41 \pm 0.05 (2)	7.44 \pm 0.13 (5)
Mg II	7.58	7.46 \pm 0.17	...	7.66 \pm 0.06 (2)	7.64 (1)
Mg I ^b			...	7.62 \pm 0.06 (2)	7.56 \pm 0.18 (4)
Mg II ^b			...	7.61 \pm 0.05 (2)	7.59 (1)
Si I	7.56	7.48 \pm 0.14	7.43 \pm 0.30 (3)
Si II	7.56	7.33 \pm 0.17	...	7.65 (1)	7.56 \pm 0.21 (2)
Ca I	6.35	6.65 \pm 0.19	6.19 \pm 0.27 (7)
Ca II	6.35	6.03 \pm 0.26	6.26 (1)
Sc II	3.10	3.13 \pm 0.20	2.69 \pm 0.36 (2)	3.03 \pm 0.25 (5)	3.22 \pm 0.24 (8)
Ti I	4.94	...	4.95 \pm 0.33 (2)
Ti II	4.94	4.86 \pm 0.25	...	4.90 \pm 0.21 (17)	5.05 \pm 0.23 (31)
Cr II	5.69	5.61 \pm 0.23	5.15 \pm 0.24 (7)	5.67 \pm 0.22 (17)	5.63 \pm 0.24 (22)
Mn II	5.53	5.81 \pm 0.20	...	5.59 (1)	5.64 (1)
Fe I	7.50	7.56 \pm 0.24	7.26 \pm 0.33 (41)	7.55 \pm 0.30 (3)	7.75 \pm 0.25 (24)
Fe II	7.50	7.40 \pm 0.11	7.23 \pm 0.23 (11)	7.46 \pm 0.22 (30)	7.48 \pm 0.22 (29)
Ni I	6.25	6.35 \pm 0.15	6.14 \pm 0.25 (4)
Y II	2.23	...	2.35 \pm 0.12 (4)	...	2.47 \pm 0.18 (2)
Ba II	2.22	2.41 \pm 0.05 (3)
Ce II	1.63	...	1.55 (1)
Nd II	1.49	...	1.80 \pm 0.40 (3)

^aOxygen abundances from syntheses (S) of the 6158 Å feature.

^bO I, Mg I, and Mg II NLTE abundances.

Table 4. Stellar Abundance Uncertainties

	A207 ΔT_{eff} +300 K	A207 $\Delta \log g$ −0.2	A207 $\Delta \xi$ −2 km s ^{−1}	41-3712 ΔT_{eff} +200 K	41-3712 $\Delta \log g$ −0.1	41-2368 ΔT_{eff} +200 K	41-2368 $\Delta \log g$ −0.1
C I	+0.20	+0.05	+0.04
O I	−0.03	−0.02	+0.08	+0.17	+0.12	+0.17	+0.07
Mg I	+0.48	+0.24	+0.51	+0.27
Mg II	+0.08	+0.08	+0.11	+0.13
Si I	+0.28	+0.08	+0.03
Si II	+0.01	+0.05	+0.02	+0.02
Ca I	+0.37	+0.08	+0.05
Ca II	+0.12	+0.01	+0.05
Sc II	+0.22	−0.02	+0.06	+0.40	+0.17	+0.40	+0.11
Ti I	+0.37	+0.06	+0.14
Ti II	+0.29	+0.12	+0.30	+0.08
Cr II	+0.13	−0.02	+0.06	+0.16	+0.07	+0.22	+0.06
Mn II	+0.11	+0.06	+0.16	+0.05
Fe I	+0.23	+0.08	+0.04	+0.44	+0.22	+0.50	+0.18
Fe II	+0.12	−0.02	+0.05	+0.12	+0.05	+0.20	+0.04
Ni I	+0.32	+0.08	+0.04
Y II	+0.25	−0.02	+0.07	+0.53	+0.16
Ba II	+0.60	+0.19
Ce II	+0.38	+0.02	+0.06	+0.60	+0.18
Nd II	+0.38	+0.02	+0.04

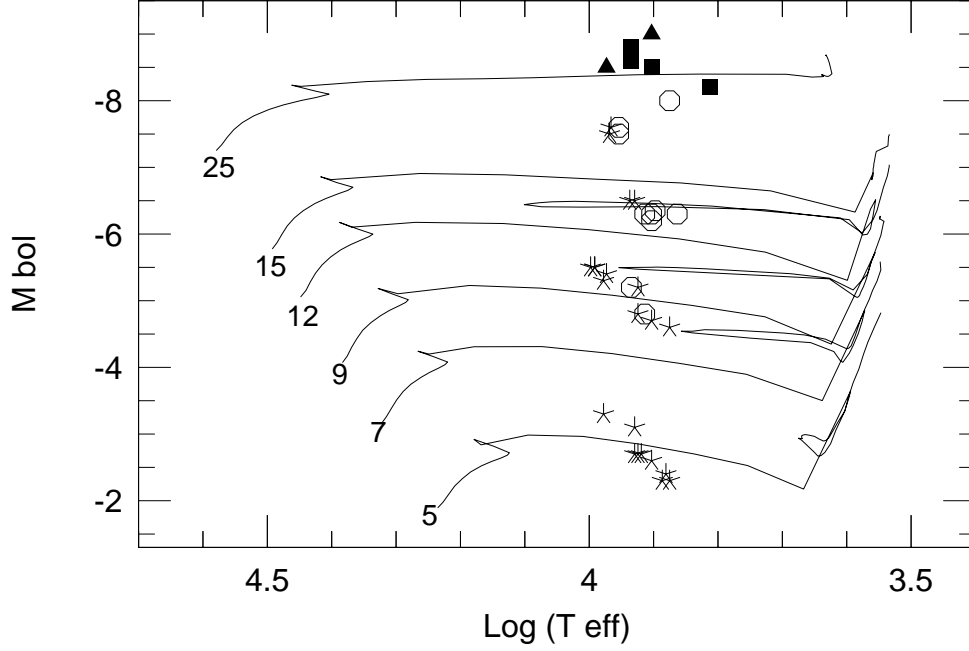


Fig. 1.— An HR diagram to show the approximate location of the four M31 A-F supergiants in this paper (*filled squares*). Also shown are 22 A-supergiants in the Galaxy (*asterisks*), 10 in the SMC (*empty circles*), and 2 in M33 (*filled triangles*) for which detailed atmospheric analyses have been published (Venn 1995b, 1999, McCarthy *et al.* 1995). Stellar evolution tracks from Schaller *et al.* (1992) are shown, with stellar masses labelled.

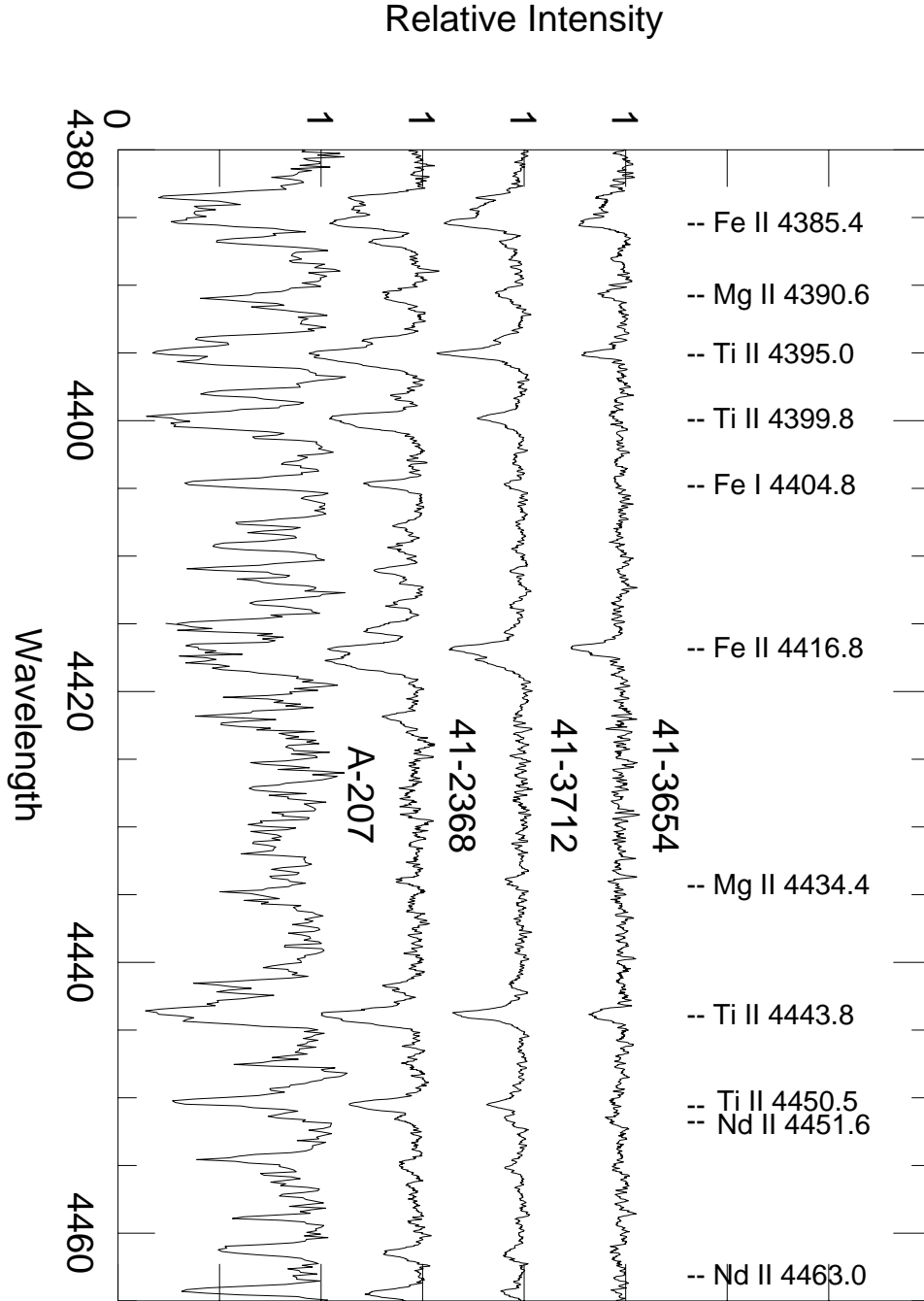


Fig. 2.— Sample spectra near 4400 Å. A few lines are identified, particularly Mg II lines used in the atmospheric analyses, as well as two Nd II features in A-207.

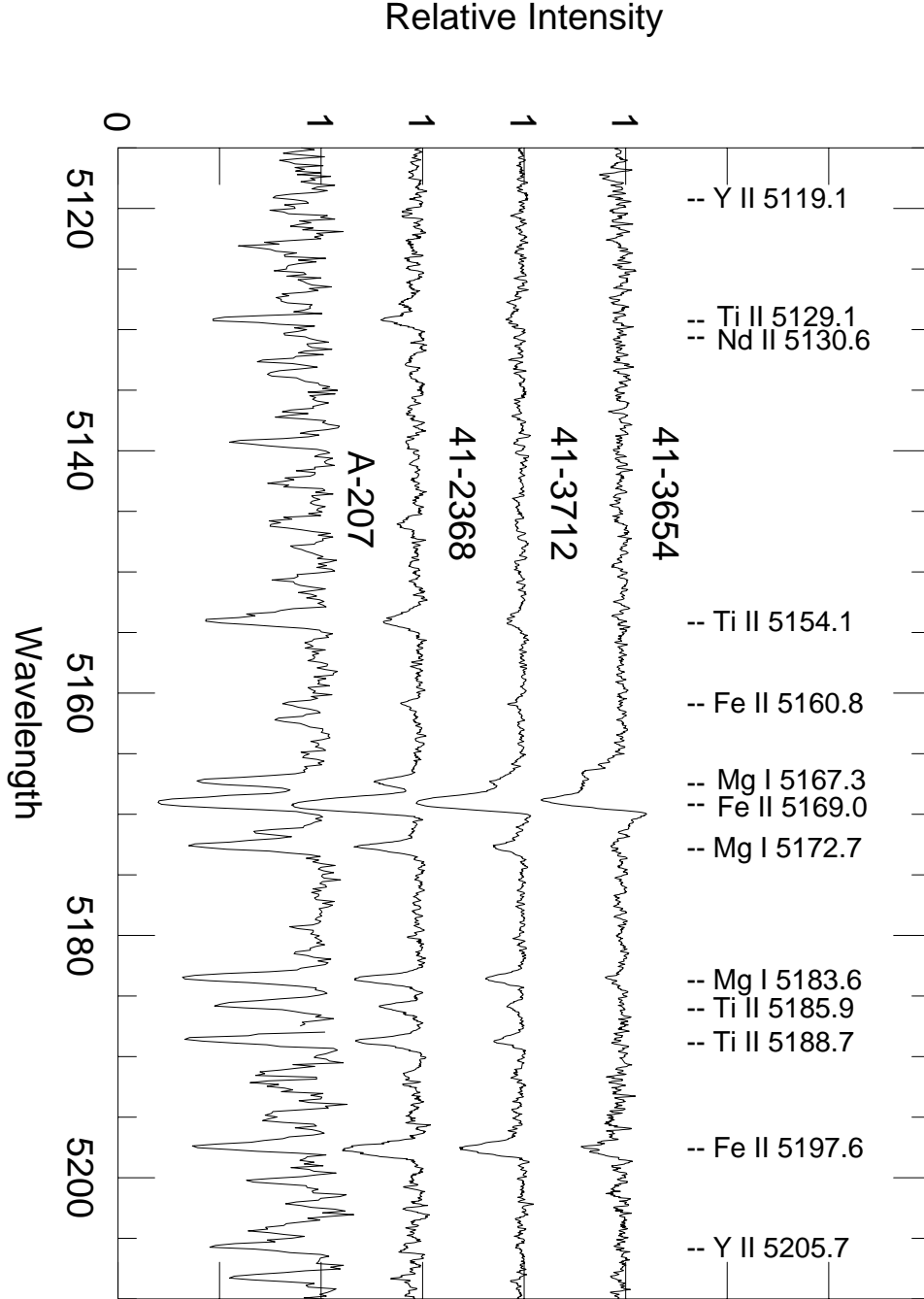


Fig. 3.— Sample spectra near 5200 Å. A few lines are identified, particularly Mg I lines used in the atmospheric analyses, as well as a Nd II and two Y II features in the cooler stars.

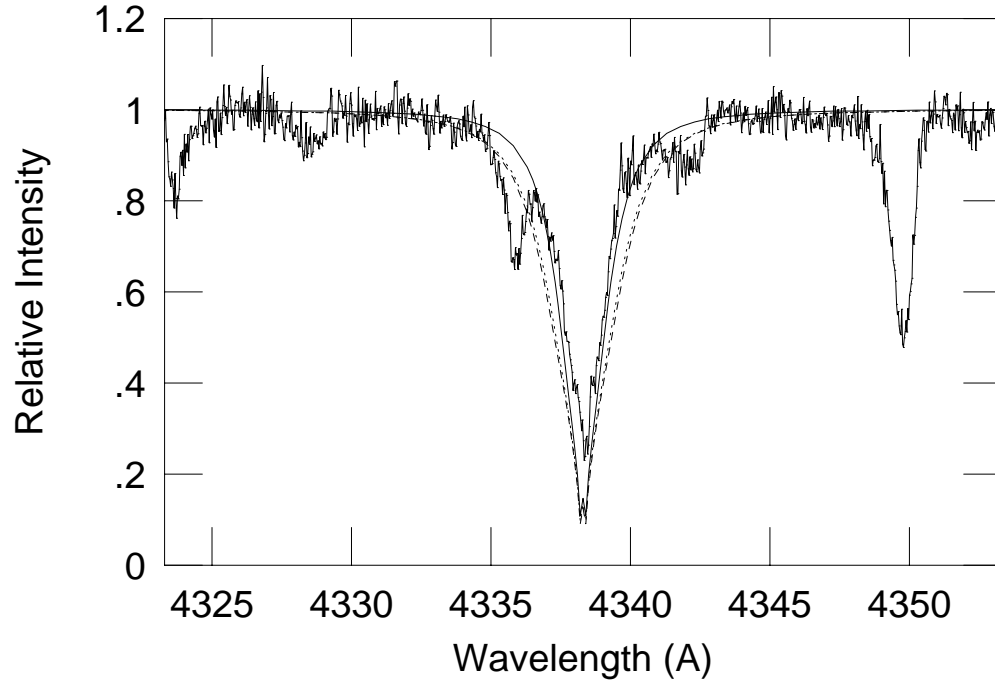


Fig. 4.— $H\gamma$ line fits for 41-3712, including the best fit from a model with $T_{\text{eff}}=8400$, $\log g=0.9$ (*solid line*), as well as $T_{\text{eff}}=8200$, $\log g=0.9$ (*dashed line*) and $T_{\text{eff}}=8400$, $\log g=1.0$ (*dotted line*).

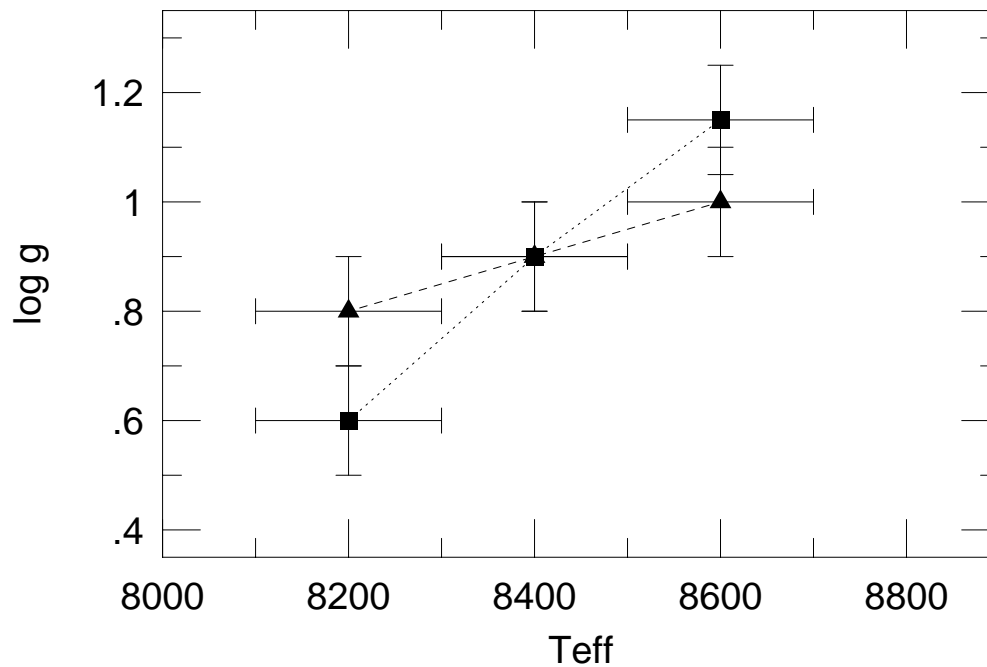


Fig. 5.— Atmospheric parameter determination for 41-3712. Mg I/Mg II is shown by *filled squares* connected by a *dotted line*. H γ fit parameters are shown by *filled triangles* connected by a *dashed line*. The model parameters at the intersection point have been adopted for this analysis.

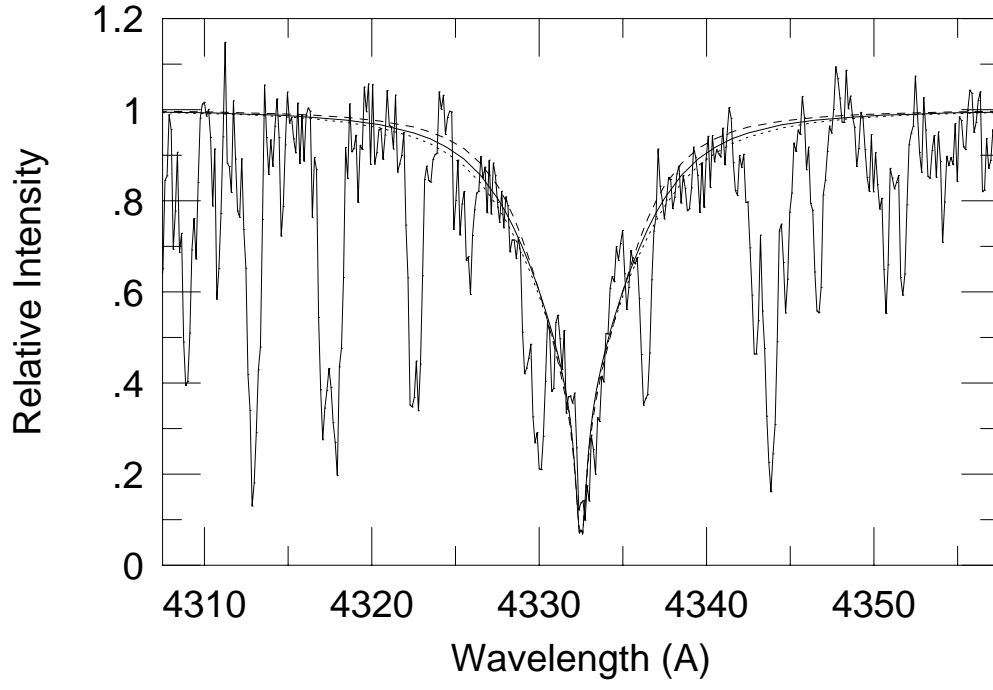


Fig. 6.— H γ line fits for A-207, including the best fit from a model with $T_{\text{eff}}=6700$, $\log g=0.2$ (*solid line*), as well as $T_{\text{eff}}=6700$, $\log g=0.3$ (*dotted lines*), and $T_{\text{eff}}=7000$, $\log g=0.3$ (*dashed line*).

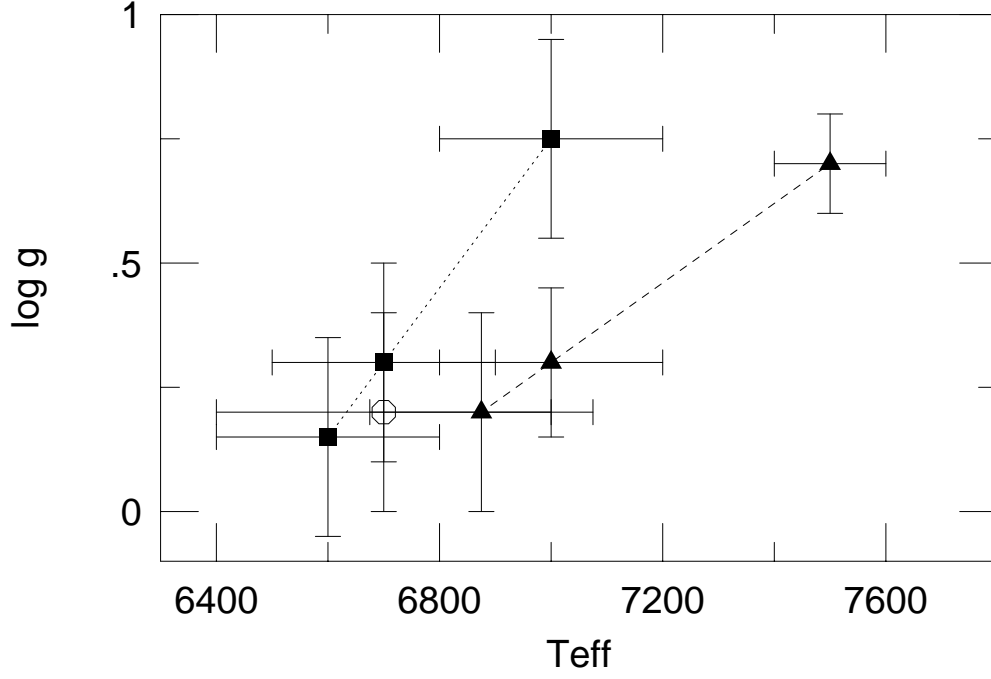


Fig. 7.— Atmospheric parameter determination for A-207. Mg I/Mg II is shown by *filled squares* connected by a *dotted line*. $H\gamma$ fit parameters are shown by *filled triangles* connected by a *dashed line*. Model parameters adopted for this analysis are shown by the *empty circle* with the estimated uncertainties.

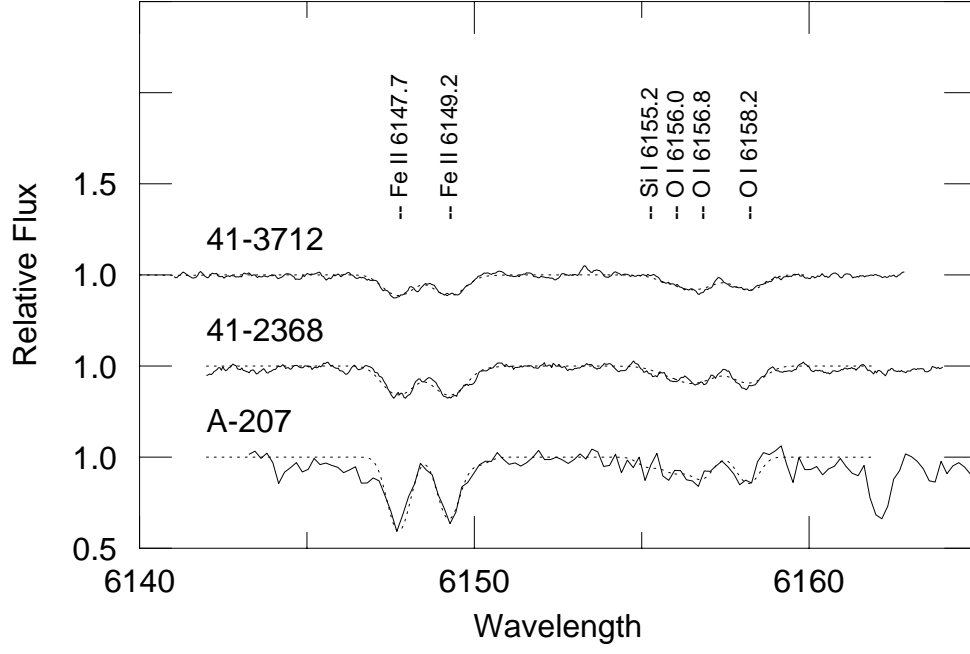


Fig. 8.— Observed O I 6158 Å feature and spectrum syntheses (*dotted line*) for our fully analysed A-F supergiants.

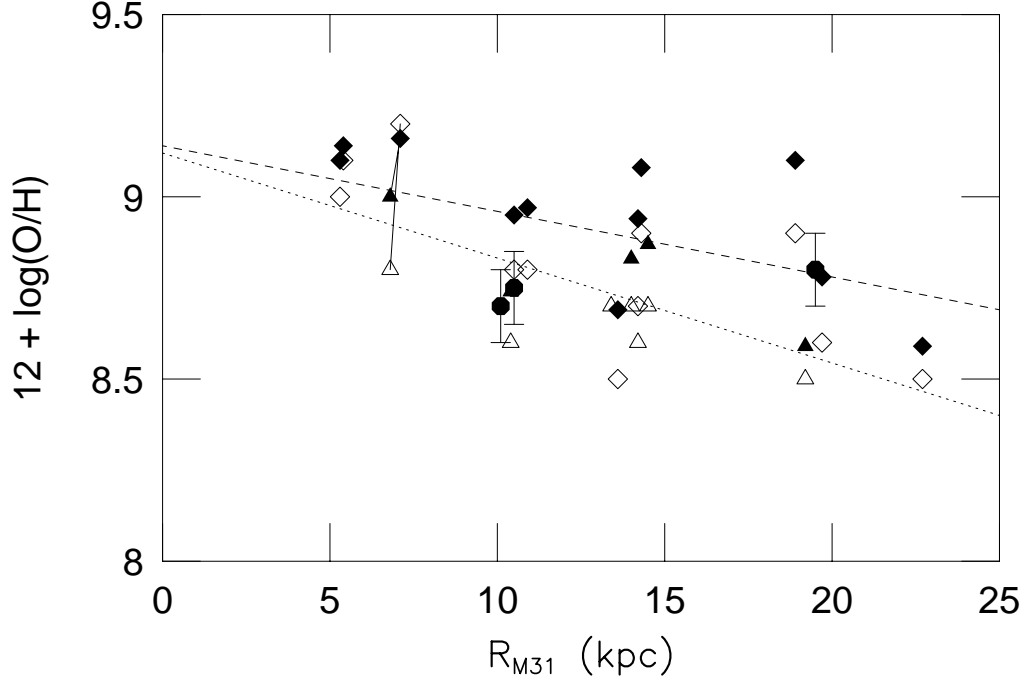


Fig. 9.— Oxygen abundances in M31 from H II regions and the three A-F supergiants in this paper. *Hollow diamonds* are the abundances from BKC82, *hollow triangles* are from Dennefeld & Kunth (1981). The *dotted line* is a least squares fit to these results. *Solid diamonds* and *solid triangles* are recalculated oxygen abundances from the data using the R_{23} calibration by ZKH94. The *dashed line* is the least squares fit to the recalibrated data. The results for one nebula, observed by both groups, is connected with a solid line (from

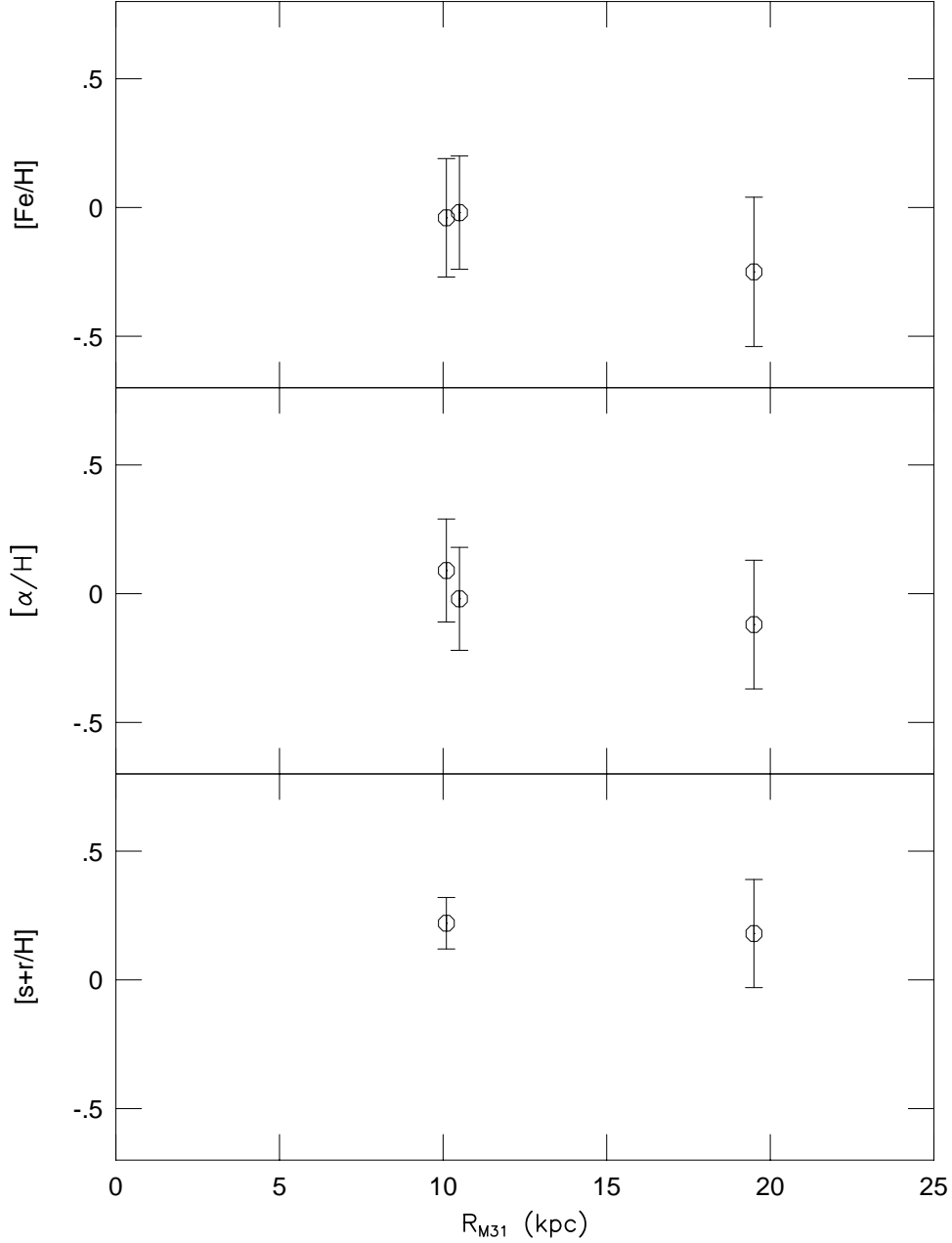


Fig. 10.— Gradients in iron, α -elements (except O), and s- and r-process elements from three A-F supergiants in M31. $[\alpha/H]$ and $[s+r/H]$ abundances are weighted means. $[Fe/H]$ is from Fe II for the two inner (and hotter) stars, while it is from Fe I & Fe II for the outer star. We note that the $[Fe/H]$ abundances plotted are within 0.01 dex of the weighted mean of all of the iron-group elements per star (excluding Fe I in the hotter stars since it is known to suffer from NLTE effects, see text).

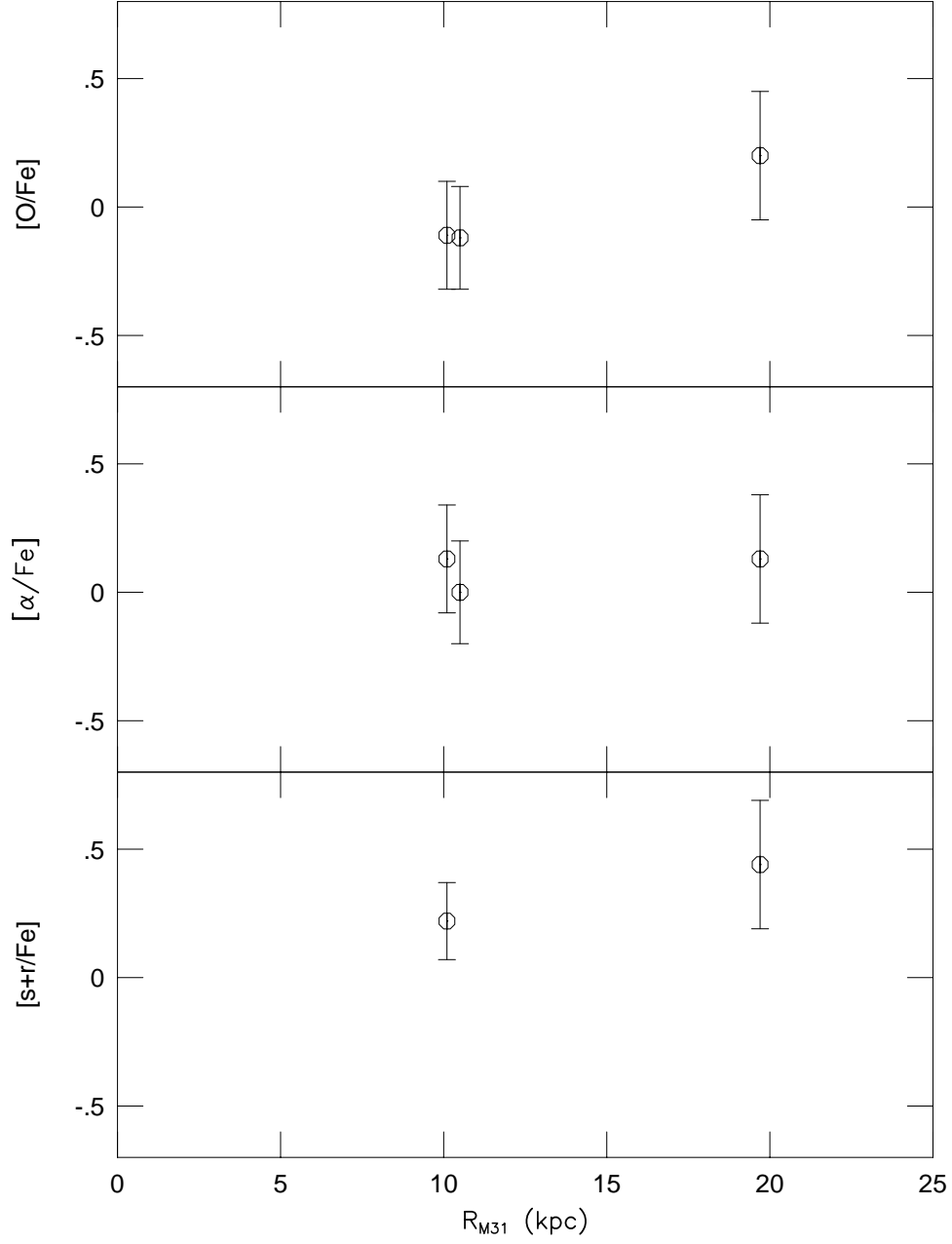


Fig. 11.— Abundance ratios $[O/Fe]$, $[\alpha/Fe]$ (without O), and $[s+r/Fe]$ from three A-F supergiants in M31. See comments on weighted mean values in Fig. 10. Note that NLTE O are used.